31st Annual International Conference of the IEEE EMBS
Minneapolis, Minnesota, USA, September 2-6, 2009

Development of a Realistic Head Model for EEG Event-Detection and Source Localization in Newborn Infants

Ivana Despotovic, Wouter Deburchgraeve, Hans Hallez, Ewout Vansteenkiste, Wilfried Philips

Abstract— **In this work we present an integrated method for electroencephalography (EEG) source localization in newborn infants, based on a realistic head model. To build a realistic head model we propose an interactive hybrid segmentation method for T1 magnetic resonance images (MRI), consisting of active contours, fuzzy c-means (FCM) clustering and mathematical morphology. Subsequently, we solve the localization problem using a spike train detection algorithm and an algorithm that deals with the forward and inverse problem. The performance of this fused method indicates that our realistic head model is suitable for the accurate localization of the EEG activity. We will present both initial qualitative and quantitative results.**

I. Introduction

EEG is a powerful tool for measuring and recording the electrical activity of the brain. Due to its non-invasiveness, it is intensively used in the diagnosis of neonatal seizures. Seizures in this study are caused by asphyxia and most commonly result in irregular activities in the EEG, like spikes. EEG source localization methods provide neurologist with the regions of the brain where spikes are generated. These methods also estimate the active anatomical zones based on the measured EEG signals and a (realistic) head model.

EEG source localization consists of two subproblems: the forward problem, that calculates the electrode potentials in a head model, given the source (usually a current dipole) and the inverse problem, that is solved by finding the dipole which best represents the given potentials at the scalp electrodes. This can be performed iteratively by modifying the dipole parameters, until, for a given set of parameters, the associated potentials (found by solving the forward problem) represent the measured potentials best. Besides the current dipole, as a model for active neurons, a volume conductor model is required to perform EEG source localization in a head model. A spike (train) detection method and potential extraction method for preterm spike EEG is proposed in [1] and an algorithm that solves both the forward and inverse problem taking into account a volume conductor model is explained in [2].

Nevertheless, an essential part in obtaining accurate source localization in the newborn brain is the selection of a head model for the forward problem. In the previous studies, simple concentric sphere models, representing different conductive layers like brain, scalp and skull, are used, in order to simplify the calculation of the forward and inverse problems. However, using a spherical instead of a realistic head model results in a dipole location error [3]–[5]. Hence, a simple (spherical) head model in the highly underdeveloped and amorphic newborn brain, can produce inaccurate source localization. Thus, it is necessary to develop a realistic head model, which is the subject of the present paper.

Both the needed MRI segmentation to build a realistic head model as well as the entire localization chain, will be explained in this study and applied to a specific subject. The paper is organized as follows: In Section II the proposed MRI segmentation, spike train detection and source localization methods are explained. Results and a discussion are given in Section III. Finally, Section IV concludes this paper.

II. Method

A. MRI segmentation

In comparison to an adult head, segmentation of preterm MRI volumes is a more complex and challenging task. The difficulties are mainly caused by: an underdeveloped brain and skull, large intensity overlaps between different tissues, intensity inhomogeneity, low contrast to noise ratio, motion artifacts (ghosting effects) and low inter-slice resolution. To date, many MRI segmentation techniques have been reported for the adult and neonatal brain [6]–[9]. The most popular methods include clustering techniques, such as expectation-maximization (EM) algorithms and fuzzy c-means (FCM) clustering.

For the purpose of realistic head modeling, we present a hybrid segmentation algorithm that combines active contours, FCM clustering and mathematical morphology. Due to the low inter-slice resolution, each slice is processed separately and the head is segmented into five labels: skin, fat, skull, cerebrospinal fluid (CSF) and brain tissue. White and gray matter are segmented as one class (brain tissue), because of the same conductivity for the neonatal brain.

The proposed algorithm is implemented in the five following steps (see Fig. 1):

Step 1: Segmentation of the head and the background using active contours [10].

Step 2: Extraction of the neonatal brain. Although there are many different solutions developed for adult brain extraction (BSE - Brain Surface Extractor, BET - Brain Extraction Tool, etc.), none of them satisfy our need. Therefore, the free ITK-SNAP software is used to delineate brain from head manually.

I. Despotovic, H. Hallez, E. Vansteenkiste, W. Philips are with Faculty of Electrical Engineering, Ghent University, MEDISIP-IPI-IBBT, Sint-Pietersnieuwstraat 41, 9000 Ghent, Belgium

W. Deburchgraeve is with the Department of Electrical Engineering, KULeuven, ESAT/SISTA, Kasteelpark Arenberg 10, 3001 Heverlee, Belgium

e-mail: ivana.despotovic@telin.ugent.be

978-1-4244-3296-7/09/$25.00 ©2009 IEEE

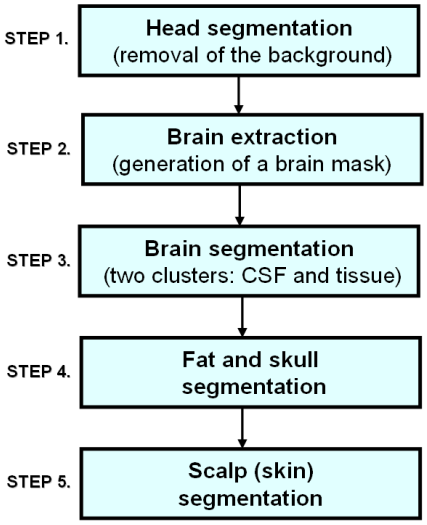

Fig. 1. Outline of the proposed MRI segmentation algorithm.

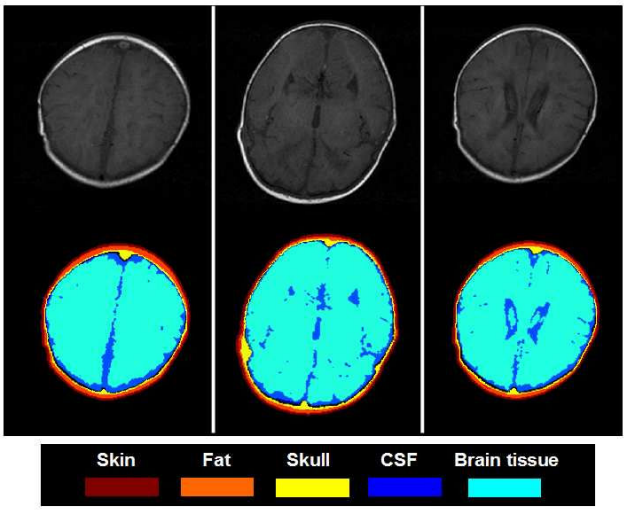

Fig. 2. Segmentation result of the head of a 39 weeks old infant. Upper row shows original T1 MRI images and the lower row presents the segmented images. At the bottom is given explanation of the labels.

Step 3: Brain segmentation into two clusters, CSF and brain tissue, using a FCM segmentation algorithm with adaptive enhancement [9], [11]. First, in order to increase the performance of the algorithm (validity and speed of convergence) and to generate a fast and reliable estimator of the FCM's parameters (i.e. the centers of the clusters and the membership degree function), an intensity-based thresholding is used [12]. Next, pixels are classified using an unsupervised FCM clustering method, that is based on minimizing the following objective function:

$$J_{\mathrm{m}}(U,V:X)=\sum_{i=1}^{C}\sum_{k=1}^{n}(u_{ik})^{m}(\|\mathbf{x}_k-\mathbf{v}_i\|)^2 \qquad (1)$$

$X=\{\mathbf{x}_k\}_{k=1}^{n}\subset R^q$ is a data matrix, q is the dimension of each $\mathbf{x}_k$ feature vector, and n is the number of feature vectors (pixel number in the image). The parameter m controls the fuzzyness of the resulting partition, and $m=2$ is used in this study. $U=[u_{ik}]$ is a $C\times n$ matrix, where u_{ik} is the membership function of vector $\mathbf{x}_k$ belonging to the i-th cluster. The membership function satisfies $u_{ik}\in[0,1]$ and $\sum_{i=1}^{C}u_{ik}=1$, $(k=1,2,...,n)$. $V=\{\mathbf{v}_i\}_{i=1}^{C}$ is the set of feature cluster centers and C is the number of clusters. The membership function and the cluster centers are given by:

$$u_{ik}=\Big[\sum_{j=1}^{C}(\|\mathbf{x}_k-\mathbf{v}_i\|/\|\mathbf{x}_k-\mathbf{v}_j\|)^{\frac{2}{m-1}}\Big]^{-1} \qquad (2)$$

$$\mathbf{v}_i=\sum_{k=1}^{n}(u_{ik})^{m}\mathbf{x}_k\ /\ \sum_{k=1}^{n}(u_{ik})^{m}\ ,(i=1,2,...,C) \qquad (3)$$

where $\|\mathbf{x}_k-\mathbf{v}_i\|=d^2(\mathbf{x}_k-\mathbf{v}_i)$ is the Euclidian norm, that measures the similarity between $\mathbf{x}_k$ and $\mathbf{v}_i$. In our algorithm, the feature vector is the pixel intensity ($q=1$).

The FCM algorithm iteratively optimizes J_{m}, by updating U and V until $\max_{i\in[1,C]}\|\mathbf{v}_i^{(l)}-\mathbf{v}_i^{(l+1)}\|_\infty<\epsilon$, where l is the number of iterations and $\|\cdot\|_\infty$ is the maximum norm. Once the final U is obtained, we apply a de-fuzzification of the fuzzy clusters $\{F_i\}_{i=1}^{C}$ into its crisp version $\{H_i\}_{i=1}^{C}$ as follows: $\mathbf{x}_k\in H_i$, if $\max_{j\in[1,C]}(u_{jk})=u_{ik}$.

Subsequently a locally adaptive enhancement is performed as follows: for pixels whose maximum membership degrees are considered too low (less then 0.8), a median filter in a local 3×3 neighborhood is used to remove noise, enhance the edges and increase the homogeneity within each region. Afterwards, the FCM clustering is rerun to achieve a more robust and accurate segmentation.

Step 4: Segmentation of the fat and skull using the same FCM algorithm applied to the images with the brain tissue extracted. Since the skull and the sinus regions are assumed to have the same electrical conductivity properties, they are segmented as the same tissue type.

Step 5: Scalp (skin) reconstruction by selecting all pixels between the edge of the head and fat using a morphological dilation with a circular structuring element of a radius one.

The final segmentation result of the proposed algorithm is shown in Fig. 2 applied to the head of a 39 weeks old infant.

At this point, when different compartments of the brain are obtained, appropriate conductivities have to be attached to them. As conductivities for the adults do not hold for the neonates, we turn to literature [13]. The conductivity of scalp, skull, CSF and brain tissue is chosen to be 0.43 S/m, 0.2 S/m, 1.43 S/m and 0.17 S/m, respectively. The electrode positions are subsequently localized on the head model using a standard 10-20 system with 6 extra temporal electrodes (see Fig. 3).

B. EEG-spike train detection

To detect the spikes in the neonatal EEG, we use our spike train detection algorithm described in [1]. This detection algorithm basically consists of three consecutive steps. In a

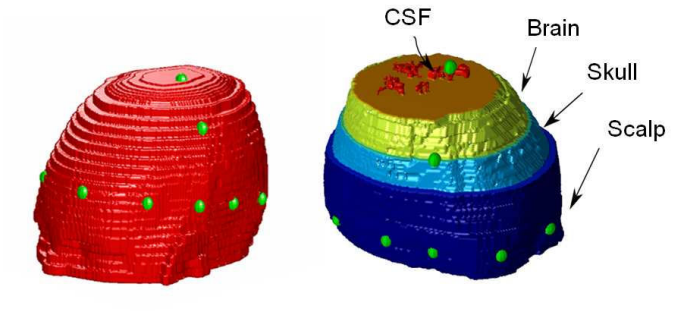

Fig. 3. Realistic head model with electrode localizations. Due to low resolution between slices (0.7mm×0.7mm×4mm), the head has a step-shaped layout.

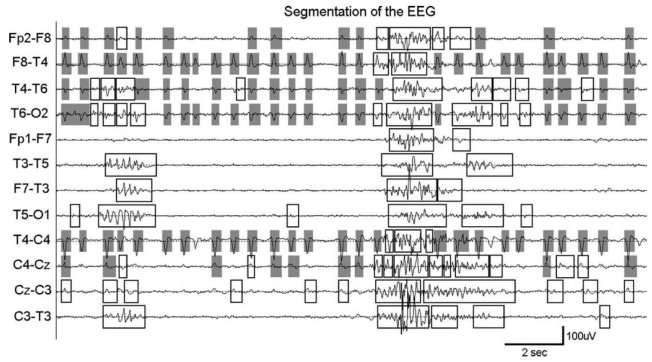

Fig. 4. Example of spike train detection: All marked segments (grey-shaded + delimited by rectangle) are detected by the segmentation step. After applying the spikiness operator and correlation analysis, only the shaded segments remain. Only these segments having a high correlation with previous segments (shaded) are detected as being part of a spike train type seizure.

first step, high energetic parts of the EEG are segmented using a Non Linear Energy Operator (NLEO) [14]. This operator is proportional to the square of both the immediate frequency and amplitude. Because of these properties, the NLEO amplifies the high-frequency spikes of the spike train relative to the background EEG, facilitating the segmentation.

The second step (see Fig. 4) analyzes the spikiness of the detected high energetic segments. This spikiness defines that the spikes need to be 'isolated' in the EEG by comparing the energy of the detected segment with its immediate background activity. The final step is the correlation analysis. To detect the occurrence of a repetitive pattern of segments, a correlation scheme was developed that grows a set of highly correlated segments. If more than 6 correlated segments are detected, the segments are classified as spikes of a spike train type seizure. The output of the algorithm is a set of highly correlated, high energetic spike-like segments corresponding to the spikes of the neonatal seizure. Finally, all detected spikes are averaged and the potential distribution over all channels at the top of the maximum peak is used as input to the source localization.

C. Source localization

As mentioned in the introduction the dipole source localization problem consists of a forward and inverse problem. By solving the forward problem, we obtain the electrode potentials caused by a dipole source. This can be done by solving Poisson's equation in the realistic head model:

$$\nabla \cdot (\sigma(\mathbf{x})V(\mathbf{x})) = I\delta(\mathbf{r}-\mathbf{r}_k) - I\delta(\mathbf{r}-\mathbf{r}_l) \qquad (4)$$

where $\sigma(\mathbf{x})$ is the location dependent conductivity tensor and $V(\mathbf{x})$ is the potential distribution inside the head model due to a dipole with current source and sink at positions $\mathbf{r}_k$ and $\mathbf{r}_l$.

In spherical head models, equation (4) can be solved using an analytical expression. In realistic inhomogeneous head models numerical methods are needed. In this study we use a finite difference method that can incorporate anisotropic conductivities [2]. Using the head model with the labeled voxels, a cubic computational grid is defined to the vertices at the edges of the voxels. Differentiating (4) in anisotropic media leads to the following finite difference formulation at each vertex $\mathbf{r}_0$:

$$I = \sum_{i=1}^{8} A_i V(\mathbf{r}_i) - \Big(\sum_{i=1}^{8} A_i\Big) V(\mathbf{r}_0) \qquad (5)$$

where $V(\mathbf{r}_i)$ is the potential at vertex $\mathbf{r}_i$ neighboring to $\mathbf{r}_0$, A_i is a coefficient that is calculated from the conductivity tensors from the voxels. I represents the current source and sink at $\mathbf{r}_k$ and $\mathbf{r}_l$. To each node, we can assign an equation according to (5). This results in a system of equations with N unknowns, with N equal to the number of nodes in the head model: $AV = I$. In our head model N was equal to approximately 2500000. To solve the system of equations, we used successive over-relaxation. Furthermore, reciprocity was used to speed up the forward calculation in the inverse problem.

Solving the inverse problem consists of finding the parameters of the dipole source that best explain the set of measured potentials consisted of the preprocessed EEG-spike trains. We find the optimal dipole position $\mathbf{r}_{opt}$ and components $\mathbf{d}_{opt}$ for the input potentials V_{in} at k scalp electrodes. This is done by minimizing the relative residual energy (RRE):

$$RRE = \frac{\|V_{in} - V_{model}(\mathbf{r},\mathbf{d})\|_2^2}{\|V_{in}\|_2^2} + C(\mathbf{r}) \qquad (6)$$

where V_{in} are the preprocessed spike trains and V_{model} are the electrode potentials obtained by solving the forward problem with a dipole source position r and components d. $\|.\|_2$ indicates the L_2-norm. $C(\mathbf{r})$ is zero for dipole positions in the brain compartment (cortical shell, white matter shell and thalamic shell) and is set to a high value elsewhere. This additional term will restrict the solution of the inverse solver to the brain compartment. The Nelder-Mead simplex method is used to find the minimum of the RRE.

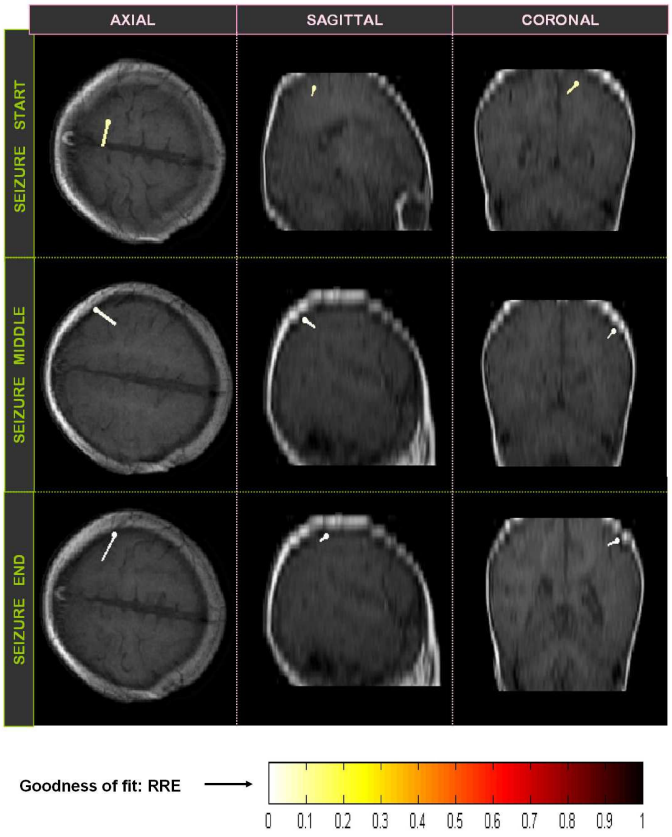

Fig. 5. Dipole representations of a burst localization. Up, middle and bottom rows show the start, middle and the end of the seizure respectively. The columns present axial, sagittal and coronal view, while the color bar shows the RRE.

III. Results

Both the MRI as well as the EEG-data in this study were recorded at the Sophia Children's Hospital (Erasmus Medical Center, Rotterdam, the Netherlands), on a newborn preterm (born at 39 weeks of gestation) subject to asphyxia. T1 MRI images were acquired on a Siemens 1,5T MRI scanner ($256\times256\times20$ voxel matrix with a resolution of $0.7\text{mm}\times0.7\text{mm}\times4\text{mm}$). Concerning EEG, a reduced 1-20 set of electrodes (13 electrodes: Fp1,2, C3,4, Cz, F7, 8, T3, 4, T5, 6, O1, 2) was used. The measurement started within 24 hours of birth at a sampling frequency of 256Hz. The seizures were scored by an experienced clinical neurophysiologist. Before analysis, the data was filtered between 0.3Hz and 30Hz.

The given data sets are processed using our method. Fig. 5 shows the qualitative results of the source localization of a burst, i.e. a seizure that begins in one place and spreads to another. Both the location and orientation of the seizure, are initialized and shown (as a dipole source). Also, the relative residual energy (RRE) is represented as the color of the dipole. The whiter the dipole is represented, the better the fit is.

Our results show very low RRE-values ($< 1\%$), which indicates that our models are suitable for the localization of the EEG activity. Also, there is a clear indication that the seizure is moving along the cortex from the beginning to the end of the seizure. When presenting these results to the expert physician, he scored this seizure behavior as highly plausible and acceptable. We are aware that a continued phase of quantitative validation is needed by testing the algorithm on more patients as well as to other clinical ground truth data. However, at the time being the latter was not to our disposal yet.

IV. Conclusion

The aim of this study is to show the feasibility to perform EEG source localization on the newborn brain, based on a realistic head model. We presented a hybrid segmentation technique to build this head model combined with two of our already existing techniques. Although our initial results are qualitative in nature, we showed that our method have very low RRE scores, which indicates that our model is a good model for this type of brain activity.

References

[1] W. Deburchgraeve, P.J. Cherian, M. De Vos, R.M. Swarte, J.H. Blok, G.H. Visser, P. Govaert, and S. Van Huffel, "Automated neonatal seizure detection mimicking a human observer reading eeg," *Clin Neurophyiol*, vol. 19, pp. 2447–2454, 2008.

[2] H. Hallez, B. Vanrumste, P. Van Hese, Y. D'Asseler, I Lemahieu, and R. Van de Walle, "A finite difference method with reciprocity used to incorporate anisotropy in electroencephalogram dipole source localization," *Physics in Medicine and Biology*, vol. 50, pp. 3787–3806, 2005.

[3] H. Buchner, T.D. Waberski, M. Fuchs, H.A. Wischmann, M. Wagner, and R. Drenckhahn, "Comparison of realistically shaped boundary-element and spherical head models in source localization of early somatosensory evoked potentials," *Brain Topography*, vol. 8, no. 2, pp. 137–143, Dec 1995.

[4] B. Yvert, O. Bertrand, M. Thevenet, J. F. Echallier, and J. Pernier, "A systematic evaluation of the spherical model accuracy in eeg dipole localization," *Electroencephalography and Clinical Neurophysiology*, vol. 102, pp. 452–459, 1997.

[5] B. Roth, A. Gorbach, and S. Sato, "How well does a three-shell model predict positions of dipoles in a realistically shaped head?," *Electroencephalography and Clinical Neurophysiology*, vol. 87, pp. 175–184, 1993.

[6] M. Prastawa, J.H. Gilmore, W. Lin, and G. Gerig, "Automatic segmentation of mr images of the developing newborn brain," *Med Image Anal*, vol. 9, no. 5, pp. 457–466, Oct 2005.

[7] K. Van Leemput, F. Maes, D. Vandermeulen, and P. Suetens, "Automated model-based tissue classification of mr images of the brain.," *IEEE Trans Med Imaging*, vol. 18, no. 10, pp. 897–908, Oct 1999.

[8] D.L. Pham and J.L. Prince, "Adaptive fuzzy segmentation of Magnetic Resonance Images," *IEEE Transactions on Medical Imaging*, vol. 18, no. 9, pp. 737–752, 1999.

[9] J.-H. Xue, A. Pižurica, W. Philips, E. Kerre, R. Van de Walle, and I. Lemahieu, "An integrated method of adaptive enhancement for unsupervised segmentation of mri brain images," *Pattern Recognition Letters*, vol. 24, pp. 2549–2560, 2003.

[10] T.F. Chan and L.A. Vese, "Active contours without edges," *IEEE J IP*, vol. 10, no. 2, pp. 266–277, Feb. 2001.

[11] J.C. Bezdek, *Pattern Recognition with Fuzzy Objective Function Algorithms*, Plenum Press, New York, 1981.

[12] S.S. Reddi, S.F. Rudin, and H.R. Keshavan, "An optical multiple threshold scheme for image segmentation," *IEEE Trans. System Man Cybernet.*, vol. 14, pp. 661–665, 1984.

[13] A. Gibson, R. H. Bayford, and D. S. Holder, "Two-dimensional finite element modelling of the neonatal head," *Physiological Measurement*, vol. 21, no. 1, pp. 45–52, Feb 2000.

[14] J.F. Kaiser, "On a simple algorithm to calculate the energy of a signal," in *IEEE Int Conf Acoust Speech Signal Process*, 1990, pp. 381–384.